Cardiomyocyte STIM1 downregulation exacerbates post-Myocardial Infarction remodeling by dysregulating mitochondrial ultrastructure and metabolic signaling

Marine Cacheux PhD, Juan Velasco MD, Xiaohong Wu MD, Benjamin Strauss PhD, and Fadi G. Akar, PhD[1]

Department of Internal Medicine, Section of Cardiovascular Medicine, Yale School of Medicine, New Haven, CT

Department of Biomedical Engineering, Yale University Schools of Engineering and Applied Sciences, New Haven, CT

Running Title: Cardiomyocyte STIM1 expression regulates post-MI remodeling

Word Count: 7744

Address correspondence to:

Fadi G. Akar, PhD
Professor of Medicine & of Biomedical Engineering
Yale University Schools of Medicine,
Engineering and Applied Sciences
Electro-biology and Arrhythmia Therapeutics Laboratory
300 George Street, 793 - 748C
New Haven CT 06511

ABSTRACT

Background: Loss of stromal interaction molecule 1 (STIM1) expression in smooth muscle cells protects against ischemia-reperfusion (I/R) injury. Whether and how decreased STIM1 expression in cardiomyocytes (CM) impacts cardiac remodeling in response to I/R injury remains unknown.

Objective: To examine mechanisms by which decreased CM-STIM1 expression in the adult heart modulates cardiac function before and after I/R injury.

Methods: 8-week old mice underwent cardiotropic AAV9-mediated gene transfer of shRNA directed against STIM1 (shSTIM1). Control (Ctrl) mice underwent shRNA luciferase or PBS injections. Ctrl and shSTIM1 mice were then challenged by 30-min coronary occlusion to induce MI, *in-vivo*. Mechanical, structural and electrophysiological (EP) properties were compared 1-week following MI. In a second cohort of mice, the impact of CM-STIM1 knockdown *per se* on upstream metabolic signaling, mitochondrial ultrastructure, and electrophysiological properties were studied.

Results: CM-STIM1 expression was markedly decreased in shSTIM1 vs Ctrl hearts. Challenge with *in-vivo* I/R injury resulted in more pronounced ($p<0.0001$) LV dysfunction indexed by % drop in fractional shortening in shSTIM1 (44.3%) vs Ctrl (12.2%) hearts 1-week post-MI. Similarly, post-MI structural remodeling and the extent of fibrosis were more severe in shSTIM1 vs Ctrl despite comparable infarct size ($p=0.514$). Consistently, shSTIM1 exhibited greater impairment in post-MI EP function including predisposition to spatially-discordant action potential alternans. To understand mechanisms underlying this differential remodeling, we examined the impact of CM-STIM1 downregulation on mitochondrial ultrastructure and regulation by metabolic signaling. Quantification of mitochondrial morphology revealed smaller, more rounded mitochondria caused by CM-STIM1 downregulation *per se*. Underlying these changes was a marked (by 55%, $p=0.0057$) increase in phosphorylated (p)DRP1 at S616 along with reduced OPA1 expression. Mitochondrial alterations were associated with significant decreases in AMPK downstream signaling with loss of phosphorylated-to-total Raptor and ACC expression in shSTIM1-vs-Ctrl hearts consistent with impaired fatty acid oxidation. These MI-independent metabolic alterations coincided with higher pro-arrhythmic vulnerability under conditions of elevated heart rate.

Conclusions: Our findings reveal that decreased CM-STIM1 expression exacerbates post-MI remodeling likely by altering metabolic processes and mitochondrial network dynamics. Functionally, STIM1-dependent mitochondrial alterations impact EP function during conditions of elevated heart rate even without the confounding influence of MI.

Key Words: Stromal Interaction Molecule 1, Myocardial Infarction, Arrhythmia, Calcium, Alternans

ABBREVIATIONS

STIM1: Stromal Interaction Molecule 1

SOCE: Store-operated calcium entry

SR/ER: Sarco/endoplasmic reticulum

VT/VF: ventricular tachycardia/ventricular fibrillation

AAV9: Adeno-associated viral vector

Ctrl: Control

MI: Myocardial Infarction

Ctrl+MI: post-MI heart

shSTIM1+MI: post-MI heart that underwent AAV9-mediated STIM1 silencing

PCL: Pacing cycle length

APD: Action potential duration

CV: Conduction velocity

Cx43: Connexin-43

FS: Fractional shortening

LVIDd: Left ventricular Internal Dimension during diastole

LVIDs: Left ventricular Internal Dimension during systole

IVSd: Intraventricular Septum diameter in diastole

IVSs: Intraventricular Septum diameter during in systole

LVPWd: Left ventricular posterior wall dimension in systole

LVPWs: Left ventricular posterior wall dimension in diastole

INTRODUCTION

STIM1 is a single-pass transmembrane protein that functions as a luminal calcium (Ca^{2+}) sensor in the endoplasmic reticulum (ER).[1,2] When ER Ca^{2+} stores are depleted, STIM1 activates the canonical process of store-operated Ca^{2+} entry (SOCE) by interacting with plasma membrane partners, primarily Orai1, to facilitate Ca^{2+} influx from the extracellular space. Although initially identified in non-excitable cells, STIM1-dependent SOCE has been observed in skeletal,[3] smooth muscle cells,[4] and cardiomyocytes.[5,6]

In cardiomyocytes, STIM1 expression is highly dependent on the developmental stage of the heart as well as its pathophysiological state. STIM1 is robustly expressed in neonatal hearts, where SOCE plays a fundamental role in the regulation of signaling involved in normal cardiac growth.[5] In contrast, STIM1 levels are reduced in healthy adult myocytes which are reliant on traditional Ca^{2+} cycling proteins (namely, voltage-gated L-type Ca^{2+} channels, SERCA2a, Phospholamban, Ryanodine Receptor Type 2, and Na-Ca exchanger) for fueling Ca^{2+} fluxes that underlie excitation-contraction coupling on a beat-by-beat basis. Of note, re-expression of STIM1 in response to pressure overload appears to play an essential role in the development of cardiomyocyte hypertrophy, both *in-vivo* and *in-vitro*.[7,8] In this regard, cardiac-specific STIM1 overexpression in a transgenic mouse model was found to promote the development of pathological cardiac hypertrophy and heart failure by enhancing SOCE,[6,9,10] effects that were abrogated by SOCE inhibition.

While STIM1 overexpression promotes pathological hypertrophy, its haploinsufficiency is also associated with abnormal cardiac function.[11] This highlights the notion that STIM1 plays a complex homeostatic role in the heart - one that requires tight regulation of its expression within a narrow physiological window. Indeed, beyond its classic SOCE-dependent effects, STIM1 is now increasingly recognized for its role in regulating fundamental cellular processes that are SOCE-independent. For example, Zhao et al.[12] reported that STIM1 overexpression in rat ventricular myocytes increases SR Ca^{2+} content through direct interaction with phospholamban, a regulatory protein of SERCA2a.[12] This finding suggests that STIM1 can influence intracellular Ca^{2+} levels rapidly and independently of SOCE. This expands our understanding of its putative role in the (patho)physiology of the adult heart, where SOCE is typically dormant. Additionally, STIM1 appears to regulate sinus node function[13-15] and inter-atrial conduction,[16] suggesting potential roles in the control of cardiac electrogenesis.[14,17] We previously investigated this issue by eliciting near complete (>80%) knockdown of STIM1 levels in an inducible myocyte-restricted manner in adult mice using an αMHC (α-myosin heavy chain)-MerCreMer system.[18] Our results

demonstrated that abrupt cardiomyocyte-specific STIM1 depletion in adult mice was sufficient to cause myocardial conduction defects, Ca^{2+}-mediated afterdepolarizations, and spatially discordant action potential alternans, which promoted the onset of sustained ventricular fibrillation leading to sudden cardiac death.[18]

In recent years, STIM1 has also emerged as an important regulator of mitochondrial function and cellular metabolism.[19-22] Moreover, STIM1 was found to interact directly with the mitochondrial dynamics protein MFN2,[23] potentially influencing mitochondrial morphology and/or interactions with the sarcoplasmic reticulum through altered tethering.[24] Indeed, mice with genetic knockout of STIM1 exhibit disrupted mitochondrial morphology and altered metabolic substrate utilization. Finally, STIM1 is directly phosphorylated by the master metabolic sensor, AMPK at specific amino acid residues that impact STIM1-mediated SOCE in response to the metabolic demand of exercise.[25,26] This demonstrates bi-directional regulation of calcium sensing and metabolic signaling in the cardiomyocyte.

Owing to the role of STIM1 in the control of intracellular Ca^{2+} homeostasis and the emerging recognition of its regulation by and influence over mitochondrial and metabolic processes, we hypothesized that it likely plays an important role in ischemia/reperfusion (I/R) injury, in which Ca^{2+} overload and mitochondrial dysfunction are hallmark pathogenic features. While loss of STIM1 in smooth muscle cells was recently shown to protect against MI,[27] the role of cardiomyocyte STIM1 expression in modulation of post-MI cardiac function remained unknown. Hence, in the present study we sought to examine the role of cardiomyocyte STIM1 downregulation in pre- and post-MI cardiac function. We achieved marked downregulation of STIM1 expression in cardiomyocytes using a gene transfer approach mediated by AAV9 encoding a short hairpin directed against STIM1 (AAV9-shSTIM1) as previously validated.[10] In the first series of studies, we examined post-MI mechanical, structural and electrophysiological (EP) remodeling 1-week following I/R injury in mice with and without CM-STIM1 downregulation (**Figure 1A**). A second series of studies was performed to examine the ultrastructure and morphology of the mitochondrial network as well as changes in mitochondrial dynamics protein expression and upstream metabolic signaling and their direct EP consequences without the confounding influence of MI (**Figure 1B)**.

We found that cardiomyocyte STIM1 downregulation dramatically exacerbates post-MI mechanical, structural and EP remodeling 1-week following I/R injury. Underlying this heightened susceptibility were changes in mitochondrial architecture and metabolic signaling that were caused by CM-STIM1 downregulation *per se*. These fundamental MI-independent changes were

functionally significant as they were sufficient to alter EP properties and enhance pro-arrhythmic behavior in response to heart rate elevation.

METHODS

Primary data supporting the findings of this study are available from the corresponding author upon reasonable request. All experimental procedures complied with the *National Institutes of Health* Guide for the Care and Use of Laboratory Animals. Protocols were approved by the Institutional Animal Care and Use Committee.

AAV9-mediated in-vivo gene transfer

Recombinant AAV9.sh*Stim1* and AAV9.sh*Luc* (against luciferase) were produced as previously described.[10] 8-week old C57bl/6J male mice received $1x10^{11}$ viral genomes (vg) of AAV9.sh*Stim1* (**Supplemental Figure 1**) or AAV9.sh*Luc* or PBS by tail vein injection.

In-vivo model of I/R injury to induce MI

Four weeks following gene transfer or sham injection, mice underwent left coronary artery (LCA) ligation for 30 minutes followed by reperfusion to induce MI (**Figure 1A**). For this procedure, anesthesia was induced via a single intraperitoneal (IP) injection of a mixture containing ketamine (1 mL x 100 mg/mL), xylazine (0.1 mL x 20 mg/mL), acepromazine (0.1 mL x 10 mg/mL), and 0.9% normal saline (1 mL). Once anesthetized, the left side of the chest was shaved. The mouse was intubated with a 20G catheter and ventilated. Body temperature was maintained using a heating pad. The animal's right hind paw was secured to the surgical table, with the left hind paw taped over the right, positioning the left side of the chest upwards. The skin was disinfected with 10% povidone-iodine. An incision was made at the fourth intercostal space to access the chest, followed by opening the pericardium. The LCA was temporarily ligated at the mid-level using a 7.0 silk suture. Successful ligation was confirmed by observing tissue pallor. After 30 minutes, the ligature was released, and reperfusion was verified by the return of the apex to its normal color. The chest was closed using 6.0 silk suture. Buprenorphine (0.05 mg/kg) was administered via IP injection for analgesia. Ventilation was discontinued once spontaneous breathing resumed, and the mouse was placed on a heating pad until fully conscious. Postoperative monitoring continued daily for one week, with additional buprenorphine injections (0.05 mg/kg) provided every 12 hours for 48 hours to manage pain.

Echocardiography

Non-invasive echocardiography was performed under sedation by IP injection of up to 75mg/kg of ketamine to allow adequate restraint of the animal while maintaining a heart rate of ~600 beats per minute. The animal chest was shaved. Left ventricular (LV) wall thickness and internal diameter were measured by M-mode using a Vivid 7 echocardiography apparatus with a 13-MHz linear array probe (General Electric, New York, NY). Short-axis parasternal views of the LV at the midpapillary level were used to guide the M-mode measurements. At least three different measurements of the intraventricular septum (IVS) and LV posterior wall (LVPW) dimensions as well as the LV internal diameter (LVID) were averaged per animal in systole (s) and diastole (d). LV performance was assessed by fraction shortening (FS) measurement as follows: FS = (LVIDd – LVIDs) / LVIDd. Echocardiography measurements were performed at 3 timepoints: baseline prior to gene transfer (8 weeks of age), 4 weeks post gene transfer (12 weeks of age) and 1 week later which also corresponds to 1 week post MI surgery (13 weeks of age).

Optical action potential mapping of ex-vivo perfused hearts

Hearts were excised rapidly and perfused on a Langendorff apparatus with Tyrode's solution containing (in mM): NaCl 129, $NaHCO_3$ 24, KCL 4, $MgCl_2$ 1.0, Glucose 11, $CaCl_2$ 1.8, KH_2PO_4 1.2, pH 7.4). Perfusion pressure was maintained at ~70 mmHg by regulating coronary perfusion flow throughout the experiment. Preparations were positioned in a tissue bath gently pressed against a glass imaging window as previously described.[28 29,30] Movement was minimized by perfusion with blebbistatin. To avoid surface cooling, preparations were immersed in the coronary effluent maintained at a physiological temperature by a heat exchanger assembly. Hearts were stimulated with a pacing electrode placed on the anterior epicardial surface of the LV, mid-way between apex and base. Cardiac rhythm was monitored continuously with silver electrodes connected to an electrocardiogram amplifier. Optical action potentials were measured with an 80x80-pixel CCD camera as previously described. [28 29,30] High-resolution optical action potentials were measured simultaneously from 6,400 sites at 1ms temporal resolution during each recording. To improve signal quality, spatial binning was performed, which yielded an array of 400 (20x20) high-fidelity optical action potentials that were amenable to accurate automated analyses.

The experimental protocol consisted of pacing hearts at progressively shorter pacing cycle lengths (PCL) starting at 140ms and in decrements of 10ms up to PCL 50ms. At each PCL, the stimulus train had a duration of at least 1min. Steady-state APD and CV values were determined as previously described. [28 29,30] Repolarization times at 75% relative to the action potential amplitude were quantified and APD was defined as the temporal difference between the repolarization and activation times at each site. Local activation time at each site was defined as the maximum first derivative during the upstroke of the action potential. Velocity vectors

(magnitude and direction) were derived from the activation times of each pixel relative to those of its neighbors. CV was measured by averaging the magnitude of the velocity vectors.

Western blots

15 or 30ug of protein lysates were loaded on 4-15% tris-glycine gels (Biorad). Primary antibodies used were STIM1 (Sigma-Aldrich 6197), GAPDH (Cell Signaling 2118), DRP1 (Cell Signaling 8570), pDRP1-S616 (Cell Signaling 3455), pDRP1-S637 (Cell Signaling 4867), MFN1 (Proteintech 13798-1-AP), MFN2 (D2010) (Cell Signaling 9482), OPA1 (D6UN6) (Cell Signaling 80471), tAMPK (Cell Signaling 2532), pAMPK (Cell Signaling 2535), tACC (Cell Signaling 3661), pACC (Cell Signaling 3661), tRaptor (Cell Signaling 2280), pRaptor-S792 (Cell Signaling 2083), Cx43 (Cell Signaling 3512) and Nav1.5 (Alomone #ASC-005) were used. Secondary antibodies were species-specific horseradish peroxidase-conjugated antibodies.

Triphenyl Tetrazolium Chloride (TTC) Staining

In a subset of experiments, MI size was determined by TTC staining. For those studies, mice were re-anesthetized 24 hours after I/R injury, and their hearts were excised and mounted on a Langendorff apparatus. The hearts were perfused for 3 minutes with a buffer solution containing 118.5 mM NaCl, 4.8 mM KCl, 1.2 mM $MgCl_2 \cdot 6H_2O$, 1.2 mM KH_2PO_4, 2.5 mM $CaCl_2$, 2.1 mM $NaHCO_3$, and 5 mM HEPES (pH 7.4) at room temperature. The LCA was reoccluded using the suture left in place after reperfusion. The hearts were then frozen for 10 min at -20°C and sectioned transversely into 1 mm slices. Slices were incubated in 1.5% triphenyl tetrazolium chloride (TTC) solution at 37°C for 20 min and subsequently fixed in a 10% formaldehyde solution for 24 hours. Infarct size was quantified using *Image J* software. Ctrl (N=5) and AAV9.shSTIM1 (N=5) hearts were compared.

Trichrome Staining

Trichrome staining was performed on 7 µm thick transverse frozen sections from AAV9.shSTIM1 and Ctrl hearts 24 hours post I/R injury, following the manufacturer's standard procedure (Sigma-Aldrich HT5-1KT). Images were quantified using *Image J*. Up to 20 images per heart from Ctrl (N = 5) and shSTIM1 (N=4) hearts were analyzed.

Electron microscopy

Murine hearts were rapidly excised and cannulated through the aorta. Hearts were perfused for 3 min with PBS at 37°C to wash out the blood followed by a fixative solution of Glutaraldehyde 3% in 0.1M Cacodylate buffer pH7.4 (Electron Microscopy Sciences-cat#16538-15) for less than 5 min. The LV was then dissected in samples of 1mm x 2mm in dimension. LV samples were placed into the fixative buffer for 2h at room temperature and then kept overnight

at 4°C. Samples were then processed by the EM Core facility. EM Images were quantified using *Image J*.

Statistical Analyses

For discrete variables, differences between groups were evaluated by using chi-square and Fisher's exact testing. For continuous variables, the Student *t* test or analysis of variance (ANOVA) were performed. The unpaired Student *t* test was used to compare differences between 2 groups. For multiple comparisons, two-way ANOVA followed by Sidak's multiple comparisons test was used. $P<0.05$ was considered significant. Echocardiographic measurements were performed at multiple timepoints in each group to define the time-course of hemodynamic changes. For those analyses, 2-way ANOVA followed by Sidak's or Tukey's multiple comparisons testing within and across outcomes were performed. An alpha level of 0.001 was used to establish significance.

RESULTS

As mentioned above, STIM1 expression in smooth muscle cells was found to protect against I/R injury.[27] Whether and how STIM1 expression in cardiomyocytes impacts cardiac remodeling in response to I/R remained unclear. We examined this issue in mice that underwent cardiotropic AAV9-mediated gene transfer of shRNA against STIM1 (shSTIM1) versus their control (Ctrl) counterparts (**Figure 1A**). Following 4 weeks of gene transfer, cardiomyocyte STIM1 expression was markedly decreased (**Figure 2A**). Remarkably, this loss of cardiomyocyte STIM1 expression was sufficient to cause an impairment of mechanical function as indexed by fractional shortening on echocardiography (42.3 ±1.7% shSTIM1 vs 59.9 ±1.2 Ctrl, $p<0.001$) (**Figure 2B**). Concomitant with the impairment in fractional shortening was a mild increase in LV chamber dimensions during both diastole and systole 4-weeks following gene transfer (**Figure 2D-F and Suppl. Figure 2A-C**). Specifically, we found a significant increase in the LV internal diameter, LVIDd (3.32±0.1mm shSTIM1 vs 2.85 ±0.05mm Ctrl, $p<0.003$) (**Figure 2D**).

Challenge of hearts with *in-vivo* I/R injury to induce MI caused an exaggerated response in shSTIM1 versus Ctrl hearts as evidenced by a more pronounced reduction in fractional shortening (**Figure 2B-C**), a significant reduction in wall thickness indexed by IVSd and LVPWd (**Figure 2E-F**), and a major increase in LV cavity dimensions (LVIDd, **Figure 2D**) despite comparable MI size between the 2 groups (**Figure 1D**). On average, control hearts exhibited ~15% reduction in fractional shortening after 1-week of the surgical MI procedure. In sharp contrast, the decrease in post-MI fractional shortening was >40% in shSTIM1 hearts (**Figure 2C**, $p<0.0001$). Exacerbation in LV dysfunction of shSTIM1 versus Ctrl hearts was associated with ~4-fold increase in fibrosis as assessed by trichrome staining (**Figure 2G-H**) reflecting more advanced post-MI structural remodeling.

Analysis of the EP substrate using high-resolution optical action potential (AP) mapping revealed a 20% reduction in CV in post-MI shSTIM1 hearts at baseline (PCL 140ms) (**Figure 3A-B**), an effect which became even more prominent with a modest increase in pacing rate to match the *in-vivo* murine heart rate (PCL 100ms, **Figure 3C**). Impaired myocardial conduction in shSTIM1 hearts was driven, at least in part, by significant (>40%) reduction in AP upstroke velocity (**Figure 3B-C).** Moreover, post-MI shSTIM1 hearts exhibited a trend towards shorter APD_{75} by 31.5% that was driven by significant acceleration in repolarization locally within the peri-infarct zone especially at PCL 100ms (**Figure 3D-F**). Next, challenge of post-MI shSTIM1 and Ctrl hearts with rapid pacing revealed presence of spatially-discordant alternans in the majority of

shSTIM1 but not Ctrl hearts (67% shSTIM1 vs 22% Ctrl hearts, p=0.13) reflecting a more adverse EP substrate (**Figure 3G-H**).

Because STIM1 expression was previously shown to impact mitochondrial properties and metabolic substrate utilization, we tested whether their heightened susceptibility to MI-related mechanical, structural and EP dysfunction may stem from altered mitochondrial network remodeling at the time of *in-vivo* I/R challenge (**Figure 1B**). Analysis of EM images 4 weeks after AAV9-mediated STIM1 knockdown revealed a major disruption of the architecture and ultrastructural organization of the mitochondrial network, which was now composed almost entirely of rounded and disjointed organelles (**Figure 4A&B**). Underlying these ultrastructural changes in shSTIM1 hearts was remodeling of the expression and phosphorylation of mitochondrial dynamics proteins. Specifically, we found a marked increase (by 55%) in phosphorylated DRP1 at S616 (pS616-DRP1 to total DRP1 ratio, 1.55±0.11 in shSTIM1 vs 1±0.09 in Ctrl hearts, p=0.0057) (**Figure 4C&D**) along with a more moderate (by 21%) increase in pS637-DRP1 levels in shSTIM1 hearts (1.21±0.04 vs 1±0.03 in Ctrl). In addition, expression of the pro-fusion protein OPA1 was downregulated by 15.4% (84.6±2.4% vs 100±5.8% in Ctrl hearts. P<0.05) with no significant changes in MFN1 or MFN2 levels (**Figure 4E&F**).

Importantly, these mitochondrial alterations were associated with impaired AMPK downstream signaling despite no change in overall AMPK and phospho-AMPK levels in shSTIM1 hearts (**Figure 5A&B**). Specifically, we found a 30% reduction in phospho-to-total ACC levels (0.69±0.05 vs 1±0.04, p=0.0014) in shSTIM1 versus Ctrl hearts (**Figure 5A&C**). This fundamental metabolic change is consistent with an increase in malonyl-CoA synthesis and impairment in fatty acid uptake into mitochondria for oxidation. Similarly, phospho-to-total Raptor levels were downregulated by 33% (0.67±0.06 vs 1±0.04, p=0.002), further highlighting the impairment in AMPK downstream signaling (**Figure 5A&D**).

To examine the functional consequences of this mitochondria/metabolic remodeling that was elicited by CM-STIM1 downregulation *per se*, we examined EP properties in mice 4 weeks following AAV9-mediated shSTIM1 delivery in a second cohort of mice that did not undergo MI (**Figure 1B**). While we found no change in average APD_{75} values between groups (**Figure 6A**), shSTIM1 hearts exhibited significant conduction slowing (40.7 ±3cm/sec shSTIM1 vs 51.15 ±3.07cm/s Ctrl, p=0.04) as evident from the representative isochrone maps (**Figure 6B-C**). This conduction defect was unrelated to Nav1.5 expression, which was upregulated by 36% in shSTIM1 (135.6±11.7%) versus Ctrl hearts (100±9.3%). Rather, it was likely related, at least in

part, to a 22% reduction in Cx43 expression (77.7±3.46% in shSTIM1 vs 100±8.4% in Ctrl hearts) (**Figure 6D-E**).

We next hypothesized that remodeling of the mitochondrial/metabolic substrate by CM-STIM1 downregulation may be sufficient to increase pro-arrhythmic susceptibility upon further elevation of heart rate. Shown in **Figure 6F** are typical action potential responses recorded from Ctrl and shSTIM1 hearts during rapid pacing at PCL 70ms. While even and odd beats in Ctrl hearts displayed minimal variation in morphology, marked beat-to-beat differences in AP morphology and duration were clearly evident in shSTIM1 hearts signifying presence of steady-state repolarization alternans, a marker of pro-arrhythmic vulnerability. Not only was the magnitude of alternans greater in shSTIM1 compared to Ctrl hearts, the onset of alternans exhibited a clear leftward shift in heart rate towards more physiological levels, again signifying greater susceptibility of shSTIM1 hearts (**Figure 6G**). Indeed, as shown in **Figure 7A**, further acceleration in pacing rate (up to PCL 50ms) was associated with pro-arrhythmic behavior in the vast majority (9/10) of shSTIM1 but not Ctrl (1/10) hearts (**Figure 7B**, $p<0.0055$). Specifically, we found that shSTIM1 hearts were prone to either loss of 1:1 capture and/or onset of sustained episodes of VT/VF (**Figure 7C**).

DISCUSSION

The main objective of this study was to investigate the impact of cardiomyocyte STIM1 downregulation in post-MI remodeling in the adult heart. This study was motivated by strong evidence linking cardiomyocyte STIM1 (CM-STIM1) expression to the regulation of both intracellular calcium homeostasis and mitochondrial/metabolic functions - processes that are critically dysregulated in the context of I/R injury. The major findings of this report are as follows: **1.** AAV9-mediated downregulation of cardiomyocyte STIM1 expression markedly sensitizes the heart to adverse remodeling caused by *in-vivo* I/R injury. Hearts with CM-STIM1 downregulation exhibit a more pronounced reduction in fractional shortening and a significant increase in left ventricular cavity dimensions. **2.** Despite a comparable infarct size relative to controls, hearts with CM-STIM1 downregulation exhibit a fourfold increase in fibrosis by trichrome staining, and greater electrical remodeling reflecting a more advanced stage of post-MI heart failure. **3.** Underlying this heightened sensitivity are fundamental changes in mitochondrial network morphology and dynamics. Hearts undergoing AAV9-mediated STIM1 knockdown reveal clear ultrastructural evidence of mitochondrial fission driven by increased phosphorylation of DRP1 at S616, reduced expression of OPA1, and loss of AMPK downstream signaling. **4.** These metabolic alterations stemming from CM-STIM1 downregulation *per se* are accompanied by impaired conduction velocity supported by partial loss of the gap junction protein Cx43, and pro-arrhythmic behavior that follows the genesis of action potential alternans upon challenge with heart rate elevation.

AAV9-mediated STIM1 downregulation exacerbates post-MI mechanical, structural and electrophysiological remodeling

STIM1 upregulation is implicated in pathological cardiac remodeling through the activation of SOCE-dependent signaling pathways, particularly under conditions of pressure overload hypertrophy.[7,8] While stress-induced STIM1 upregulation is pathophysiological in nature, its forced downregulation through genetic manipulation is also deleterious. Indeed, we previously demonstrated that abrupt knockdown of STIM1 expression in the adult heart using a tamoxifen-inducible and cardiac-restricted strategy unmasked severe electrophysiological defects, including genesis of Ca^{2+}-mediated afterdepolarizations and heightened predisposition to inducible ventricular fibrillation *ex-vivo* and sudden cardiac death *in-vivo* within only 3-7 days of STIM1

depletion.[18] These complex effects of altered STIM1 expression (up and down) likely arise from its extensive regulatory influence on both canonical (SOCE-dependent) and non-canonical (SOCE-independent) pathways that maintain cardiac function under basal and stress conditions.

Owing to the role of STIM1 in the control of intracellular Ca^{2+} homeostasis[12,17,31] and the emerging recognition of its regulation by and influence over mitochondrial[32] and metabolic processes,[21,33,34] we hypothesized that it likely plays an important role in post-MI remodeling, in which Ca^{2+} overload and mitochondrial dysfunction are hallmark pathogenic features. Importantly, the role of STIM1 in post-MI remodeling was highlighted in a recent elegant study demonstrating that selective deletion of STIM1 in smooth muscle cells protects against I/R injury by reducing MI size and improving overall cardiac function.[27] Moreover, STIM1 upregulation following MI appears to correlate with increased apoptosis.[35] *In-vitro* studies have shown that H9C2 cells subjected to hypoxia/reoxygenation protocols exhibit a four-fold increase in STIM1 expression accompanied by a significant rise in apoptosis. Notably, suppression of STIM1 via siRNA in these cells substantially reduces apoptosis rates.[35]

These observations and others prompted our current study, which aimed to determine whether STIM1 reduction in native cardiomyocytes *in-vivo* by AAV9-mediated gene transfer would confer protection against adverse remodeling that follows I/R injury in the adult heart. Our findings demonstrate that cardiomyocyte STIM1 downregulation does not only fail to protect against post-MI remodeling but rather exacerbates it. This extends prior observations that CM-STIM1 downregulation accelerates the transition from compensated hypertrophy to decompensated heart failure in response to pressure overload.[10]

The strikingly different outcomes that are elicited by reducing STIM1 levels in cardiomyocytes versus in smooth muscle cells,[27] highlight the critical need to define the divergent cell type-specific roles of STIM1 within the heart. These disparate outcomes caution against the use of nonspecific STIM1 inhibitors, given the contrasting effects that STIM1 inhibition can elicit in different cardiac cell populations that contribute to the pathophysiology of I/R injury. Collectively, our study and that of Mali et al.[27] emphasize the necessity of delineating distinct STIM1-dependent pathophysiological mechanisms to enable the development of targeted, cell-specific therapeutic strategies.

Loss of cardiomyocyte STIM1 expression causes remodeling of mitochondrial ultrastructure and metabolic signaling

Given the marked exacerbation of post-MI remodeling observed upon cardiomyocyte STIM1 downregulation, we next sought to elucidate the underlying mechanisms. We hypothesized that reduced STIM1 expression might induce broad mitochondrial and/or metabolic remodeling, thereby compounding the impact of I/R injury. This hypothesis was informed by emerging evidence from several studies linking STIM1 to mitochondrial function[22,36] and metabolic regulation, both in the heart[21] and in skeletal muscle. [37]

Using an AAV9-mediated short hairpin RNA approach to downregulate STIM1 in the adult heart *in-vivo*, we first observed significant remodeling of mitochondrial ultrastructure and morphology, as assessed by electron microscopy imaging. Specifically, mitochondria exhibited smaller, more rounded profiles with reduced area and perimeter, changes that coincided with increased expression of phosphorylated DRP1 at S616 and reduced OPA1 levels, indicative of heightened mitochondrial fission. Similarly, Collins et al.[22] reported an increased number of smaller mitochondria, also linked to mitochondrial fission. In a follow-up study, these authors further explored the effects of STIM1 deficiency on cardiac metabolism in cardiac restricted (Cr) STIM1-KO mice.[21] They found that by 20 weeks of age these mice exhibited fundamental shifts in metabolic substrate utilization (namely reduced reliance on glucose), alongside decreased expression of glucose transporter 4 and reduced phosphorylation of AMPK. Although fatty acid oxidation rates remained unchanged, lipid and triglyceride levels were elevated, along with increased expression of proteins involved in fatty acid metabolism, suggesting an imbalance between fatty acid uptake and oxidation.[21] Whether these changes were directly caused by loss of STIM1 *per se* or were secondary to broad gene reprograming during cardiac development remained unknown. A major advantage of our experimental approach was the ability to avoid potentially confounding factors associated with long-term compensatory gene reprogramming in standard transgenic models. Indeed, we found that mitochondrial perturbations that are unmasked by AAV9-mediated downregulation of STIM1 expression in the adult heart were also accompanied by significant remodeling of key metabolic pathways highlighting the impact of STIM1 *per se* on these processes. Specifically, we found a decrease in AMPK downstream signaling, evidenced by reduced phospho-to-total ratios of ACC and Raptor, despite preserved total AMPK protein expression. These observations suggest potential impairment in fatty acid oxidation, consistent with findings in (Cr)STIM1-KO mice. Taken together, those findings highlight the notion that AMPK signaling not only impacts STIM1-mediated SOCE[34] but is also highly regulated by it; thereby impacting mitochondrial and metabolic homeostasis in the adult heart.

STIM1 downregulation in the adult heart alters metabolic, mechanical and electrophysiological properties to promote stress-induced arrhythmias

In our present study we induced CM-STIM1 downregulation in the adult heart to avoid widescale compensatory gene reprogramming and assessed cardiac function at baseline (time of gene delivery) and 4 weeks later. This allowed us to examine the impact of STIM1 on basal cardiac function before induction of MI. Our findings of impaired LV mechanical function and chamber remodeling in AAV9-shSTIM1 hearts are consistent with findings by Benard et al.[10] using a similar approach. Collectively, our present data and those of Benard et al.[10] and Collins et al[22] highlight the notion that reduced STIM1 levels in the heart are sufficient to impair cardiac function even without imposition of an external stressor such as transaortic constriction or I/R injury.

As mentioned above, defects in mechanical function as a consequence of CM-STIM1 downregulation coincided with remodeling of the mitochondrial network. A major advance of our present study was the systematic identification of the electrophysiological consequences of this remodeling without the confounding influence of MI. We found that AAV9-mediated STIM1 downregulation was sufficient to cause significant myocardial conduction slowing, driven at least in part by reduced Cx43 expression. This finding highlights a previously unrecognized link between STIM1, an ER/SR calcium sensor, and Cx43, a critical intercalated disc protein. Future studies are needed to determine whether this link arises from direct regulation of Cx43 expression by STIM1 or through secondary metabolic pathways that may impact Cx43 synthesis and/or degradation. Furthermore, we found that STIM1 downregulation *per se* heightened susceptibility of hearts to pro-arrhythmic behavior that was preceded by the genesis of action potential alternans. These findings are reminiscent of our previous observations in mice with abrupt cardiomyocyte-specific STIM1 depletion using a tamoxifen-inducible cardiac-restricted STIM1 knockdown (STIM1-KD) strategy.[18]

Conclusions

The data presented here demonstrate that cardiomyocyte STIM1 downregulation exacerbates the response of the heart to I/R injury by impairing mitochondrial ultrastructure and AMPK-mediated signaling. These mitochondria/metabolic defects that stem directly from CM-STIM1 downregulation are sufficient to alter EP properties and predispose hearts to proarrhythmic behavior independent of MI.

Sources of Funding:

This work was supported in part by National Institutes of Health grants to FGA (R01HL149344, R21HL165147, R01HL148008, R01HL163092, and R21HL114378)

Conflict of Interest Disclosures: None

REFERENCES

1. Rosenberg P, Katz D, Bryson V. SOCE and STIM1 signaling in the heart: Timing and location matter. *Cell calcium*. 2019;77:20-28. doi: 10.1016/j.ceca.2018.11.008
2. Sallinger M, Grabmayr H, Humer C, Bonhenry D, Romanin C, Schindl R, Derler I. Activation mechanisms and structural dynamics of STIM proteins. *J Physiol*. 2024;602:1475-1507. doi: 10.1113/JP283828
3. Sztretye M, Geyer N, Vincze J, Al-Gaadi D, Olah T, Szentesi P, Kis G, Antal M, Balatoni I, Csernoch L, et al. SOCE Is Important for Maintaining Sarcoplasmic Calcium Content and Release in Skeletal Muscle Fibers. *Biophys J*. 2017;113:2496-2507. doi: 10.1016/j.bpj.2017.09.023
4. Kassan M, Ait-Aissa K, Radwan E, Mali V, Haddox S, Gabani M, Zhang W, Belmadani S, Irani K, Trebak M, et al. Essential Role of Smooth Muscle STIM1 in Hypertension and Cardiovascular Dysfunction. *Arteriosclerosis, thrombosis, and vascular biology*. 2016;36:1900-1909. doi: 10.1161/ATVBAHA.116.307869
5. Voelkers M, Salz M, Herzog N, Frank D, Dolatabadi N, Frey N, Gude N, Friedrich O, Koch WJ, Katus HA, et al. Orai1 and Stim1 regulate normal and hypertrophic growth in cardiomyocytes. *Journal of molecular and cellular cardiology*. 2010;48:1329-1334. doi: 10.1016/j.yjmcc.2010.01.020
6. Troupes CD, Wallner M, Borghetti G, Zhang C, Mohsin S, von Lewinski D, Berretta RM, Kubo H, Chen X, Soboloff J, et al. Role of STIM1 (Stromal Interaction Molecule 1) in Hypertrophy-Related Contractile Dysfunction. *Circulation research*. 2017;121:125-136. doi: 10.1161/CIRCRESAHA.117.311094
7. Luo X, Hojayev B, Jiang N, Wang ZV, Tandan S, Rakalin A, Rothermel BA, Gillette TG, Hill JA. STIM1-dependent store-operated Ca(2)(+) entry is required for pathological cardiac hypertrophy. *Journal of molecular and cellular cardiology*. 2012;52:136-147. doi: 10.1016/j.yjmcc.2011.11.003
8. Ohba T, Watanabe H, Murakami M, Sato T, Ono K, Ito H. Essential role of STIM1 in the development of cardiomyocyte hypertrophy. *Biochemical and biophysical research communications*. 2009;389:172-176. doi: 10.1016/j.bbrc.2009.08.117
9. Correll RN, Goonasekera SA, van Berlo JH, Burr AR, Accornero F, Zhang H, Makarewich CA, York AJ, Sargent MA, Chen X, et al. STIM1 elevation in the heart results in aberrant Ca(2)(+) handling and cardiomyopathy. *Journal of molecular and cellular cardiology*. 2015;87:38-47. doi: 10.1016/j.yjmcc.2015.07.032
10. Benard L, Oh JG, Cacheux M, Lee A, Nonnenmacher M, Matasic DS, Kohlbrenner E, Kho C, Pavoine C, Hajjar RJ, et al. Cardiac Stim1 Silencing Impairs Adaptive Hypertrophy and Promotes Heart Failure Through Inactivation of mTORC2/Akt Signaling. *Circulation*. 2016;133:1458-1471; discussion 1471. doi: 10.1161/CIRCULATIONAHA.115.020678
11. Ohba T, Watanabe H, Murakami M, Iino K, Adachi T, Baba Y, Kurosaki T, Ono K, Ito H. Stromal interaction molecule 1 haploinsufficiency causes maladaptive response to pressure overload. *PloS one*. 2017;12:e0187950. doi: 10.1371/journal.pone.0187950
12. Zhao G, Li T, Brochet DX, Rosenberg PB, Lederer WJ. STIM1 enhances SR Ca2+ content through binding phospholamban in rat ventricular myocytes. *Proceedings of the National Academy of Sciences of the United States of America*. 2015;112:E4792-4801. doi: 10.1073/pnas.1423295112
13. Liu J, Xin L, Benson VL, Allen DG, Ju YK. Store-operated calcium entry and the localization of STIM1 and Orai1 proteins in isolated mouse sinoatrial node cells. *Frontiers in physiology*. 2015;6:69. doi: 10.3389/fphys.2015.00069

14. Zhang H, Graham V, Nepliouev I, Stiber JA, Rosenberg P. STIM1 interacts with HCN4 channels to coordinate diastolic depolarization in the mouse Sinoatrial node. *bioRxiv*. 2023. doi: 10.1101/2023.05.03.539287
15. Nguyen N, Biet M, Simard E, Beliveau E, Francoeur N, Guillemette G, Dumaine R, Grandbois M, Boulay G. STIM1 participates in the contractile rhythmicity of HL-1 cells by moderating T-type Ca(2+) channel activity. *Biochimica et biophysica acta*. 2013;1833:1294-1303. doi: 10.1016/j.bbamcr.2013.02.027
16. Zhang H, Bryson V, Luo N, Sun AY, Rosenberg P. STIM1-Ca(2+) signaling in coronary sinus cardiomyocytes contributes to interatrial conduction. *Cell calcium*. 2020;87:102163. doi: 10.1016/j.ceca.2020.102163
17. Zhang H, Sun AY, Kim JJ, Graham V, Finch EA, Nepliouev I, Zhao G, Li T, Lederer WJ, Stiber JA, et al. STIM1-Ca2+ signaling modulates automaticity of the mouse sinoatrial node. *Proceedings of the National Academy of Sciences of the United States of America*. 2015;112:E5618-5627. doi: 10.1073/pnas.1503847112
18. Cacheux M, Strauss B, Raad N, Ilkan Z, Hu J, Benard L, Feske S, Hulot JS, Akar FG. Cardiomyocyte-Specific STIM1 (Stromal Interaction Molecule 1) Depletion in the Adult Heart Promotes the Development of Arrhythmogenic Discordant Alternans. *Circulation Arrhythmia and electrophysiology*. 2019;12:e007382. doi: 10.1161/CIRCEP.119.007382
19. Collins HE, Zhu-Mauldin X, Marchase RB, Chatham JC. STIM1/Orai1-mediated SOCE: current perspectives and potential roles in cardiac function and pathology. *American journal of physiology Heart and circulatory physiology*. 2013;305:H446-458. doi: 10.1152/ajpheart.00104.2013
20. Collins HE, Zhang D, Chatham JC. STIM and Orai Mediated Regulation of Calcium Signaling in Age-Related Diseases. *Front Aging*. 2022;3:876785. doi: 10.3389/fragi.2022.876785
21. Collins HE, Pat BM, Zou L, Litovsky SH, Wende AR, Young ME, Chatham JC. Novel role of the ER/SR Ca(2+) sensor STIM1 in the regulation of cardiac metabolism. *American journal of physiology Heart and circulatory physiology*. 2019;316:H1014-H1026. doi: 10.1152/ajpheart.00544.2018
22. Collins HE, He L, Zou L, Qu J, Zhou L, Litovsky SH, Yang Q, Young ME, Marchase RB, Chatham JC. Stromal interaction molecule 1 is essential for normal cardiac homeostasis through modulation of ER and mitochondrial function. *American journal of physiology Heart and circulatory physiology*. 2014;306:H1231-1239. doi: 10.1152/ajpheart.00075.2014
23. Singaravelu K, Nelson C, Bakowski D, de Brito OM, Ng SW, Di Capite J, Powell T, Scorrano L, Parekh AB. Mitofusin 2 regulates STIM1 migration from the Ca2+ store to the plasma membrane in cells with depolarized mitochondria. *J Biol Chem*. 2011;286:12189-12201. doi: 10.1074/jbc.M110.174029
24. Dorn GW, 2nd, Song M, Walsh K. Functional implications of mitofusin 2-mediated mitochondrial-SR tethering. *Journal of molecular and cellular cardiology*. 2015;78:123-128. doi: 10.1016/j.yjmcc.2014.09.015
25. Stein BD, Calzolari D, Hellberg K, Hu YS, He L, Hung CM, Toyama EQ, Ross DS, Lillemeier BF, Cantley LC, et al. Quantitative In Vivo Proteomics of Metformin Response in Liver Reveals AMPK-Dependent and -Independent Signaling Networks. *Cell Rep*. 2019;29:3331-3348 e3337. doi: 10.1016/j.celrep.2019.10.117
26. Yu F, Machaca K. The STIM1 Phosphorylation Saga. *Cell calcium*. 2022;103:102551. doi: 10.1016/j.ceca.2022.102551
27. Mali V, Haddox S, Belmadani S, Matrougui K. Essential role for smooth muscle cell stromal interaction molecule-1 in myocardial infarction. *J Hypertens*. 2018;36:377-386. doi: 10.1097/HJH.0000000000001518

28. Xie C, Hu J, Motloch LJ, Karam BS, Akar FG. The Classically Cardioprotective Agent Diazoxide Elicits Arrhythmias in Type 2 Diabetes Mellitus. *Journal of the American College of Cardiology*. 2015;66:1144-1156. doi: 10.1016/j.jacc.2015.06.1329
29. Akar FG, Aon MA, Tomaselli GF, O'Rourke B. The mitochondrial origin of postischemic arrhythmias. *The Journal of clinical investigation*. 2005;115:3527-3535. doi: 10.1172/JCI25371
30. Akar FG, Yan GX, Antzelevitch C, Rosenbaum DS. Unique topographical distribution of M cells underlies reentrant mechanism of torsade de pointes in the long-QT syndrome. *Circulation*. 2002;105:1247-1253.
31. Parks C, Alam MA, Sullivan R, Mancarella S. STIM1-dependent Ca(2+) microdomains are required for myofilament remodeling and signaling in the heart. *Scientific reports*. 2016;6:25372. doi: 10.1038/srep25372
32. Ross GR, Bajwa T, Jr., Edwards S, Emelyanova L, Rizvi F, Holmuhamedov EL, Werner P, Downey FX, Tajik AJ, Jahangir A. Enhanced store-operated Ca(2+) influx and ORAI1 expression in ventricular fibroblasts from human failing heart. *Biology open*. 2017;6:326-332. doi: 10.1242/bio.022632
33. Nelson ME, Parker BL, Burchfield JG, Hoffman NJ, Needham EJ, Cooke KC, Naim T, Sylow L, Ling NX, Francis D, et al. Phosphoproteomics reveals conserved exercise-stimulated signaling and AMPK regulation of store-operated calcium entry. *EMBO J*. 2019;38:e102578. doi: 10.15252/embj.2019102578
34. Lang F, Eylenstein A, Shumilina E. Regulation of Orai1/STIM1 by the kinases SGK1 and AMPK. *Cell calcium*. 2012;52:347-354. doi: 10.1016/j.ceca.2012.05.005
35. He F, Wu Q, Xu B, Wang X, Wu J, Huang L, Cheng J. Suppression of Stim1 reduced intracellular calcium concentration and attenuated hypoxia/reoxygenation induced apoptosis in H9C2 cells. *Biosci Rep*. 2017;37. doi: 10.1042/BSR20171249
36. Nan J, Li J, Lin Y, Saif Ur Rahman M, Li Z, Zhu L. The interplay between mitochondria and store-operated Ca(2+) entry: Emerging insights into cardiac diseases. *J Cell Mol Med*. 2021;25:9496-9512. doi: 10.1111/jcmm.16941
37. Wilson RJ, Lyons SP, Koves TR, Bryson VG, Zhang H, Li T, Crown SB, Ding JD, Grimsrud PA, Rosenberg PB, et al. Disruption of STIM1-mediated Ca(2+) sensing and energy metabolism in adult skeletal muscle compromises exercise tolerance, proteostasis, and lean mass. *Mol Metab*. 2022;57:101429. doi: 10.1016/j.molmet.2021.101429

FIGURE LEGENDS

FIGURE 1: **Experimental Timeline and Major Procedures. A.** Schematic illustrating the experimental timeline, included major procedures, measurements and assays used to assess the impact of cardiomyocyte STIM1 downregulation on post-MI cardiac function. After baseline echocardiographic measurements, 8 weeks old C57Bl6 male mice underwent AAV9-mediated shSTIM1 gene transfer via a tail vein injection with $1x10^{11}$ vg. Control (Ctrl) mice received either an AAV9 carrying a short hairpin against luciferase (shLuci) or PBS injection. Four weeks post gene transfer (at 12 weeks of age), mice underwent echocardiographic measurements. They were then randomized for cardiac MI operation by surgical LCA occlusion for 30min followed by reperfusion or a sham procedure. One week post-MI or sham surgery (at 13 weeks of age), mice underwent a third round of echocardiographic measurements and were then sacrificed for ex vivo EP measurements, molecular or histological analyses. **B.** Schematic illustrating the experimental timeline, including major procedures, measurements and assays used to determine the impact of cardiomyocyte STIM1 downregulation *per se* (without MI) in altering mitochondrial ultrastructure and EP properties. **C.** Anatomical image of the mapped epicardial surface (left) and corresponding optical action potentials (AP) in a representative post-MI heart. **D**. Infarct size quantification 24 hours post MI surgery. Images of a Ctrl and a shSTIM1heart sliced post TTC staining. 6 slices from apex (left) to base are shown for each heart. Infarct size quantification shows no difference between AAV9.shSTIM1 (25.18+/-3.82%, N=5) and Ctrl (28.4+/-2.76%, N=5) hearts.

FIGURE 2: **Post-MI mechanical and structural remodeling are exacerbated by AAV9-mediated STIM1 silencing. A**. Representative western blot documenting efficiency of STIM1 downregulation in lysates from isolated cardiomyocytes of shSTIM1 versus control (PBS and shLuci injected hearts). Cardiomyocyte STIM1 expression is reduced relative to GAPDH in shSTIM1 hearts 4 weeks post gene transfer. **B-F.** Echocardiographic assessment of LV remodeling induced by AAV9-mediated STIM1 silencing before and after MI. Echocardiographic measurements were obtained at baseline (8w old), 4 weeks post gene transfer (12w old) and prior to the MI procedure, and 1 week post-MI or sham operation (13w old) in Ctrl and shSTIM1 mice. Parameters measured include fractional shortening (FS), the percent change in FS post MI (13 week versus 12 week timepoints), interventricular septum thickness (IVS), left ventricular internal diameter (LVID) and left ventricular posterior wall thickness (LVPW) during diastole (d). N=10 AAV9.shSTIM1 mice and N=9 control mice were used for this analysis. Statistics: two-ways-

ANOVA between Ctrl and shSTIM1, with SD error bars. **G**. Representative images of Masson's Trichrome staining of LV sections from Ctrl and shSTIM1 hearts, 24h post MI surgery. **H.** Quantification of interstitial fibrosis is shown indicating a 70% increase in interstitial fibrosis in post-MI shSTIM1 (shSTIM1+MI) vs Ctrl (Ctrl+MI) hearts. N=5 Ctrl+MI hearts and N=5 shSTIM1+MI hearts were used for this analysis; Up to 20 images were quantified per heart.

FIGURE 3: **Cardiomyocyte STIM1 depletion exacerbates post-MI electrical remodeling A.** Representative depolarization maps depicting the spread of activation across the ventricular epicardium of post-MI Ctrl and post-MI shSTIM1 hearts. **B**-**C.** Average and distribution of CV and upstroke velocity values for all post-MI Ctrl (Ctrl+MI) and post-MI shSTIM1 (shSTIM1+MI) hearts measured at PCL 140ms and PCL 100ms. **D.** Representative APD contour maps measured from a post-MI control (Ctrl+MI) and a post-MI shSTIM1 (shSTIM1+MI) heart. **E-F**. Quantification of APD_{75} on the entire epicardial surface (global) and within the peri-infarct region at PCL of 140ms and 100ms. N=6 Ctrl+MI and N=6 shSTIM1+MI hearts used for this analysis. **G**. Representative AP traces recorded from a post-MI shSTIM1 hearts (shSTIM1+MI) showing the emergence of beat-to-beat AP alternans at elevated pacing rates (PCL shortening). **H**. Action potential traces recorded at PCL of 70ms. Post-MI shSTIM1 hearts exhibited more severe alternans patterns that were spatially discordant compared to their post-MI Ctrl counterparts.

FIGURE 4: **Cardiomyocyte STIM1 downregulation alters mitochondrial network ultrastructure**. **A**. Transmission electron microscopy images from the left ventricles of Ctrl and shSTIM1 hearts 4 weeks post gene transfer showing differences in mitochondrial network ultrastructure and morphology. **B**. Mitochondrial dimensions (perimeters and areas) were quantified. **C-D**. Representative immunoblots and densitometric quantifications of total and phosphorylated DRP1 at Ser 637 and Ser 616 in tissue lysates from Ctrl and shSTIM1 hearts, 4 weeks post gene transfer. DRP1 protein levels were normalized to GAPDH and pDRP1 proteins were normalized to total DRP1 levels. shSTIM1 hearts showed a 55% and 21% increase in pS616/tDRP1 ratio (1.55±0.11 vs 1±0.09 in Ctrl) and p637/tDRP1 ratio (1.21±0.04 vs 1±0.03 in Ctrl), respectively versus Ctrl hearts. N=5 hearts per group was used. **E-F**. Representative immunoblots and densitometric quantifications of the major mitochondrial fission/fusion proteins, Mitofusin-1 (MFN1), Mitofusin-2 (MFN2) and OPA1 normalized to GAPDH in lysates from Ctrl and shSTIM1 hearts 4 weeks post gene transfer. While MFN1 and MFN2 protein levels were unchanged, OPA1 was decreased by 15.4% (84.6±2.4% vs 100±5.8% in Ctrl hearts). N=5 hearts

per group. Statistics: t-test. **GAPDH*** and **GAPDH#** mean that the same GAPDH blot was used to normalize the expression of multiple proteins (as indicated in Panels C and E) after stripping the membrane and blotting for those proteins.

FIGURE 5: **Cardiomyocyte STIM1 downregulation impairs AMPK downstream signaling. A.** Representative immunoblots of AMPK, phospho-AMPK-Thr172, ACC, phospho-ACC-Ser79, raptor and phospho-raptor-Ser792 from cardiac lysates of Ctrl and shSTIM1 hearts 4 weeks post gene transfer. **B-D**. Densitometric quantifications of phosphorylated-to-total ratios for AMPK, ACC, and Raptor are shown. N=5 hearts per group. Statistics: t-test.

FIGURE 6: **STIM1 silencing per se (without MI) causes conduction slowing and promotes pacing-induced alternans. A.** *Ex-vivo* optical action potential mapping measurements showed similar action potential duration (APD_{75}) in Ctrl (48.7±1.8ms) and shSTIM1 (51.4±1.4ms) hearts (N=6 Ctrl and 5 shSTIM1 hearts). **B-C**. Conduction velocity quantification and representative isochrone maps showing CV slowing in shSTIM1 hearts (40.7 ±3cm/sec vs 51.15 ±3.07cm/s in Ctrl hearts, p=0.04, PCL 140ms) (N=5 hearts per group). **D-E**. Representative immunoblots and quantification showing a significant increase in Nav1.5 and a decrease in Cx43 protein expression in shSTIM1 hearts 4 weeks post gene transfer. N=5 hearts per group. Statistics: T-test. **F**. Action potential (AP) traces recorded from representative Ctrl and shSTIM1 hearts during rapid pacing at PCL 70ms document presence of substantial beat to beat variability (alternans) in shSTIM1 but not in Ctrl hearts. **G**. STIM1 silencing per se accelerated the development of AP alternans. The PCL at which AP alternans was first observed in shSTIM1 hearts was slower than that for Ctrl heart indicative of heightened propensity.

FIGURE 7: **AAV9-mediated STIM1 silencing promotes pro-arrhythmic responses to heart rate elevation. A**. Optical action potential traces of each of the 10 Ctrl and 10 shSTIM1 hearts showing arrhythmic activity marked by either loss of pacing capture or onset of VT in the vast majority of shSTIM1 but not Ctrl hearts in response to the pacing protocol which entailed pacing from PCL 100ms to 50ms in a Δ10ms decrements. **B**. Bar graph showing the number of hearts presenting with rapid pacing (up to 50ms PCL) induced arrhythmic behavior indexed by either loss of capture (<LOC) or onset of sustained VT/VF in all Ctrl and shSTIM1 hearts. Statistical

comparison made using Fisher's exact test. **C**. Volume-conducted ECG recoding from an *ex-vivo* perfused shSTIM1 heart during showing onset of sustained VT/VF.

SUPPLEMENTAL FIGURE 1: AAV9-mediated shSTIM1 silencing vector. Sequence of shRNA targeting STIM1 and vector schematic.

SUPPLEMENTAL FIGURE 2: Echocardiographic measurements of systolic function. Echocardiographic assessment of post-MI cardiac dysfunction induced by STIM1 silencing. Echocardiographic measurements were obtained at baseline (8w old mice), 4 weeks post gene transfer (12w old) and 1 week post-MI surgery (13w old) in Ctrl and shSTIM1 mice. Parameters measured during systole: (**A**) left ventricular internal diameter (LVID), (**B**) interventricular septum thickness (IVS) and (**C**) left ventricular posterior wall thickness (LVPW). N=10 AAV9.shSTIM1 mice and N=9 Ctrl mice. Statistics: two-ways-ANOVA between Ctrl and shSTIM1, with SD error bars.

Figure 1

A Effects of shSTIM1 on post-MI

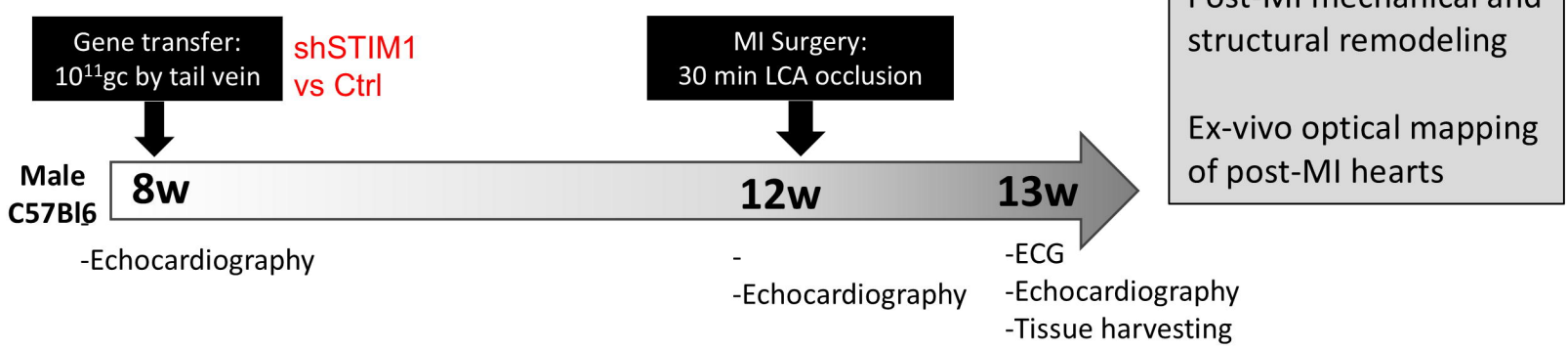

B Effects of shSTIM1 per se (before MI)

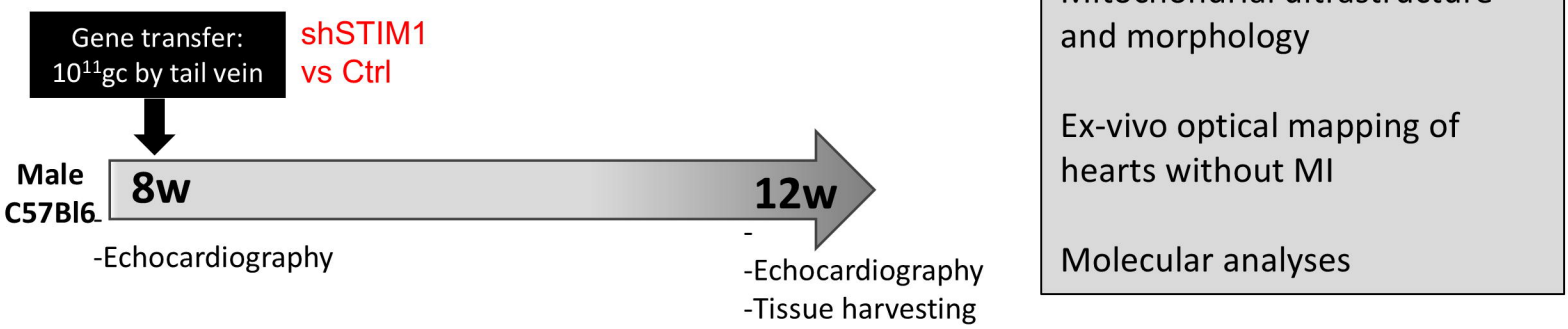

C Ex-vivo optical mapping

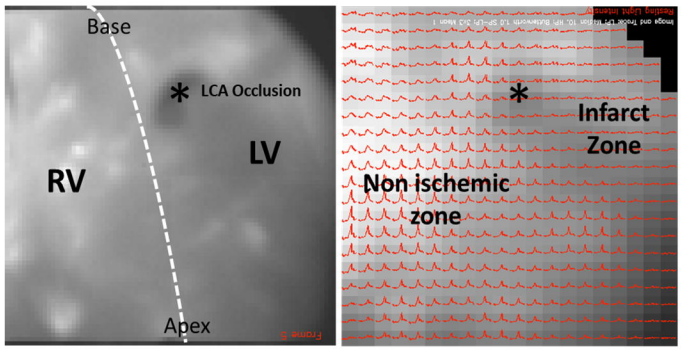

D

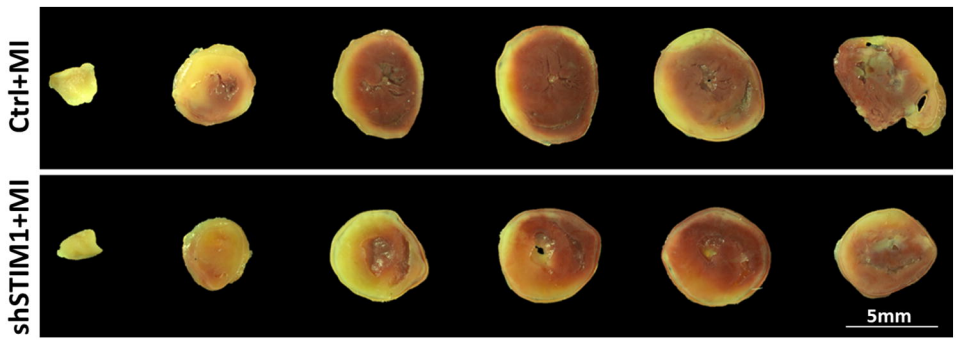

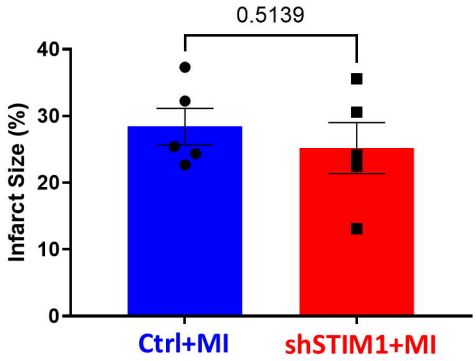

Figure 2

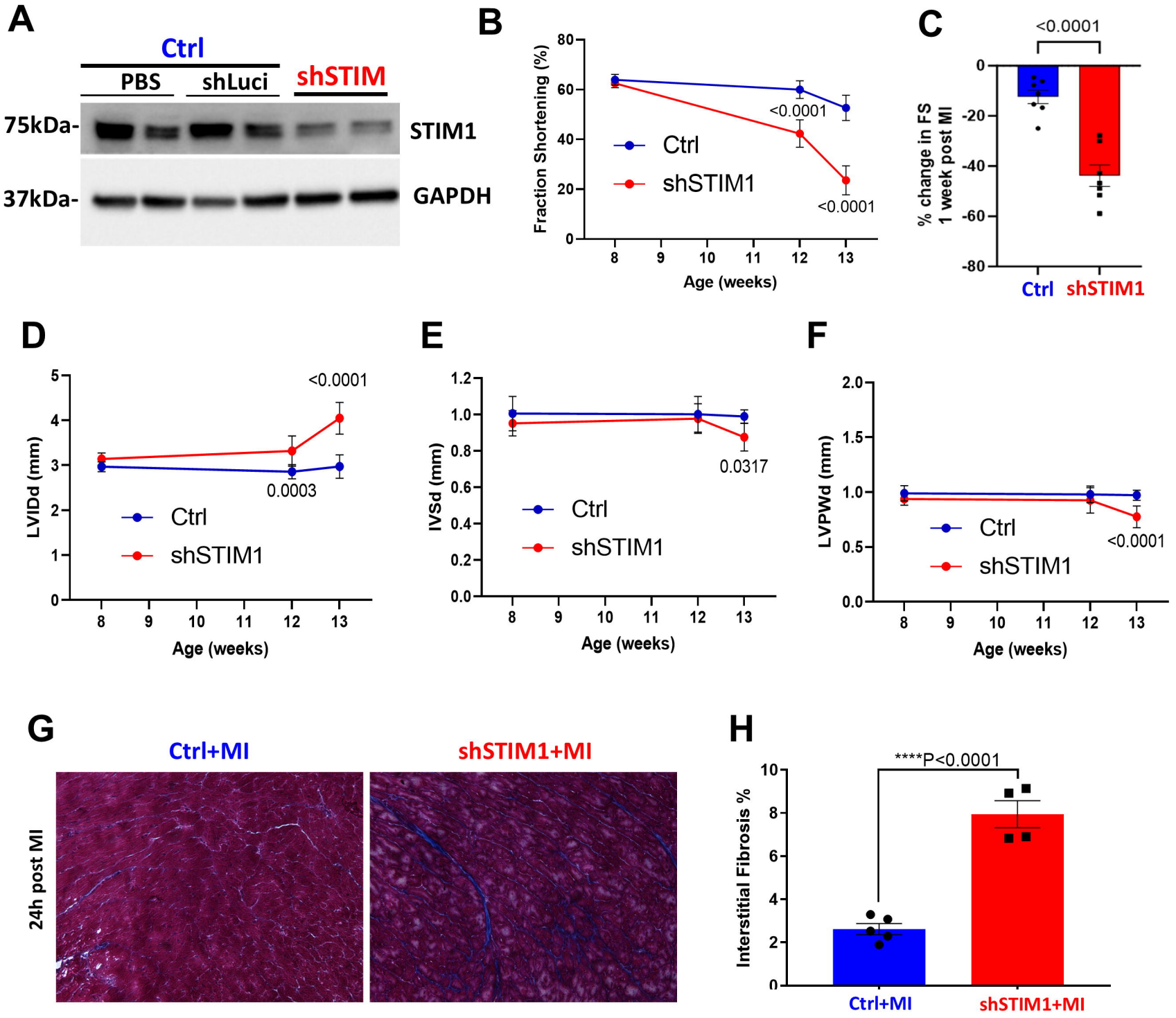
A
Ctrl
PBS
shLuci
shSTIM
75kDa-
STIM1
37kDa-
GAPDH
B
Fraction Shortening (%)
Age (weeks)
Ctrl
shSTIM1
<0.0001
<0.0001
C
<0.0001
% change in FS 1 week post MI
Ctrl
shSTIM1
D
LVIDd (mm)
Age (weeks)
Ctrl
shSTIM1
<0.0001
0.0003
E
IVSd (mm)
Age (weeks)
Ctrl
shSTIM1
0.0317
F
LVPWd (mm)
Age (weeks)
Ctrl
shSTIM1
<0.0001
G
Ctrl+MI
shSTIM1+MI
24h post MI
H
****P<0.0001
Interstitial Fibrosis %
Ctrl+MI
shSTIM1+MI

Figure 3

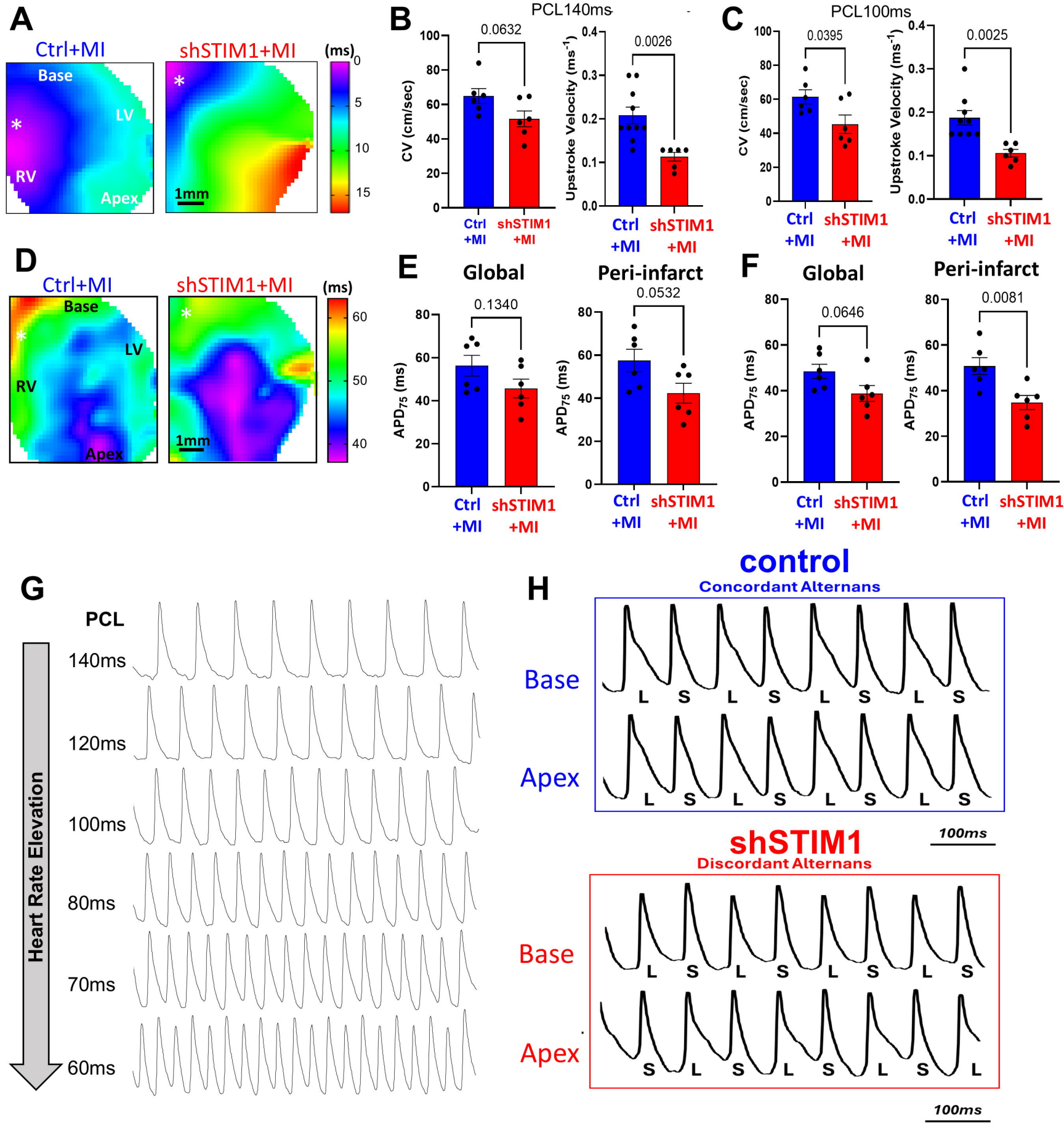
A
Ctrl+MI
shSTIM1+MI
(ms)
Base
LV
RV
Apex
1mm
0
5
10
15
B
PCL140ms
0.0632
0.0026
CV (cm/sec)
Upstroke Velocity (ms-1)
Ctrl +MI
shSTIM1 +MI
C
PCL100ms
0.0395
0.0025
D
Ctrl+MI
shSTIM1+MI
(ms)
60
50
40
E
Global
Peri-infarct
0.1340
0.0532
APD75 (ms)
F
Global
Peri-infarct
0.0646
0.0081
G
PCL
140ms
120ms
100ms
80ms
70ms
60ms
Heart Rate Elevation
H
control
Concordant Alternans
Base
Apex
L S L S L S L S
100ms
shSTIM1
Discordant Alternans
Base
Apex
L S L S L S L S
S L S L S L S L
100ms

Figure 4

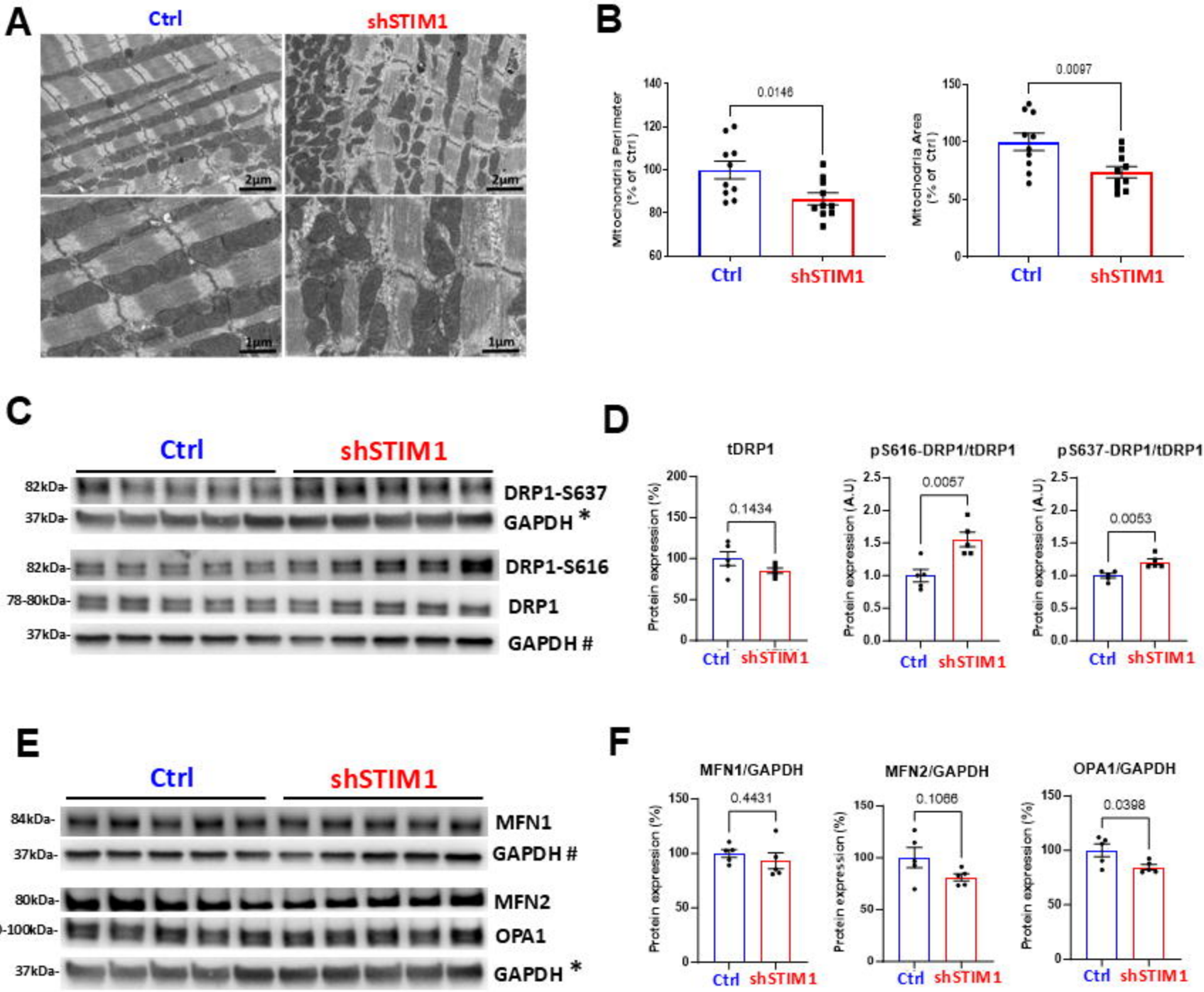
A
Ctrl
shSTIM1
2µm
2µm
1µm
1µm
B
Mitochondria Perimeter (% of Ctrl)
0.0146
Mitochondria Area (% of Ctrl)
0.0097
Ctrl
shSTIM1
C
Ctrl
shSTIM1
82kDa-
DRP1-S637
37kDa-
GAPDH *
82kDa-
DRP1-S616
78-80kDa-
DRP1
37kDa-
GAPDH #
D
tDRP1
pS616-DRP1/tDRP1
pS637-DRP1/tDRP1
Protein expression (%)
Protein expression (A.U)
0.1434
0.0057
0.0053
Ctrl
shSTIM1
E
Ctrl
shSTIM1
84kDa-
MFN1
37kDa-
GAPDH #
80kDa-
MFN2
80-100kDa-
OPA1
37kDa-
GAPDH *
F
MFN1/GAPDH
MFN2/GAPDH
OPA1/GAPDH
Protein expression (%)
0.4431
0.1066
0.0398
Ctrl
shSTIM1

Figure 5

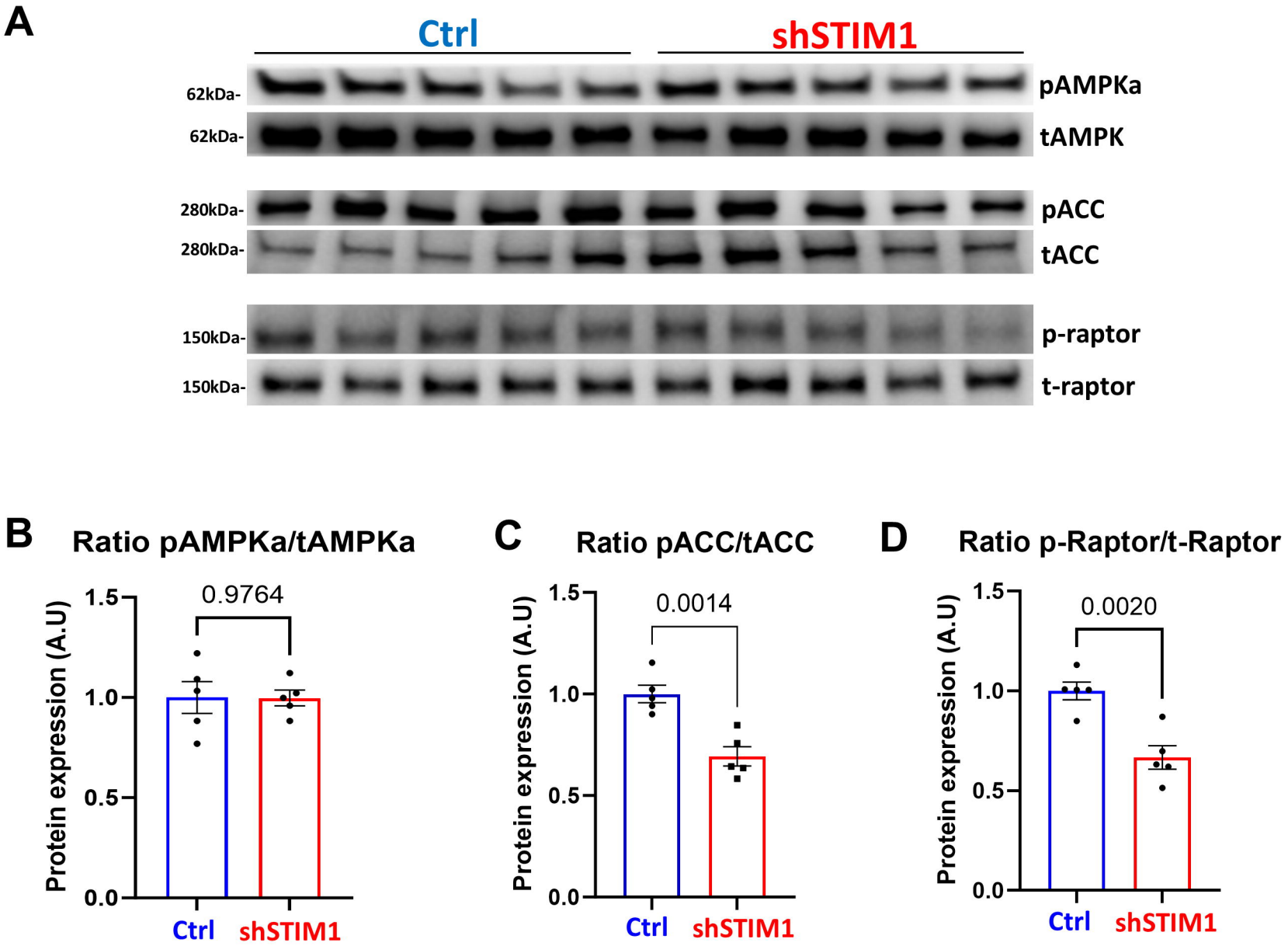
A
Ctrl
shSTIM1
62kDa-
pAMPKa
62kDa-
tAMPK
280kDa-
pACC
280kDa-
tACC
150kDa-
p-raptor
150kDa-
t-raptor
B
Ratio pAMPKa/tAMPKa
0.9764
Protein expression (A.U)
1.5
1.0
0.5
0.0
Ctrl
shSTIM1
C
Ratio pACC/tACC
0.0014
Protein expression (A.U)
1.5
1.0
0.5
0.0
Ctrl
shSTIM1
D
Ratio p-Raptor/t-Raptor
0.0020
Protein expression (A.U)
1.5
1.0
0.5
0.0
Ctrl
shSTIM1

Figure 6

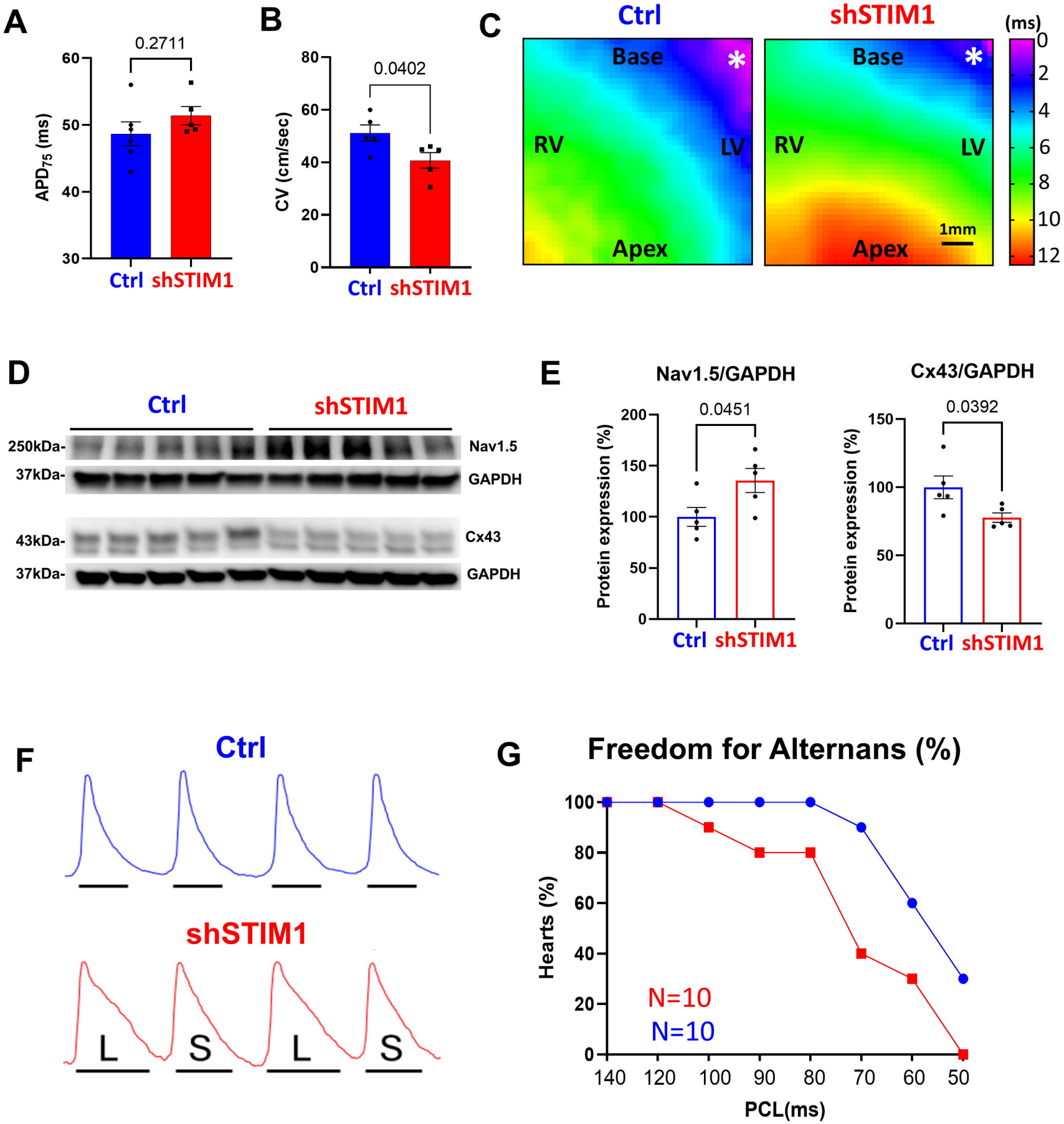
A
0.2711
APD75 (ms)
60
50
40
30
Ctrl
shSTIM1
B
0.0402
CV (cm/sec)
80
60
40
20
0
Ctrl
shSTIM1
C
Ctrl
shSTIM1
(ms)
Base
RV
LV
Apex
1mm
0
2
4
6
8
10
12
D
Ctrl
shSTIM1
250kDa-
Nav1.5
37kDa-
GAPDH
43kDa-
Cx43
37kDa-
GAPDH
E
Nav1.5/GAPDH
0.0451
Protein expression (%)
200
150
100
50
0
Ctrl
shSTIM1
Cx43/GAPDH
0.0392
Protein expression (%)
150
100
50
0
Ctrl
shSTIM1
F
Ctrl
shSTIM1
L
S
L
S
G
Freedom for Alternans (%)
Hearts (%)
100
80
60
40
20
0
N=10
N=10
140
120
100
90
80
70
60
50
PCL(ms)

Figure 7

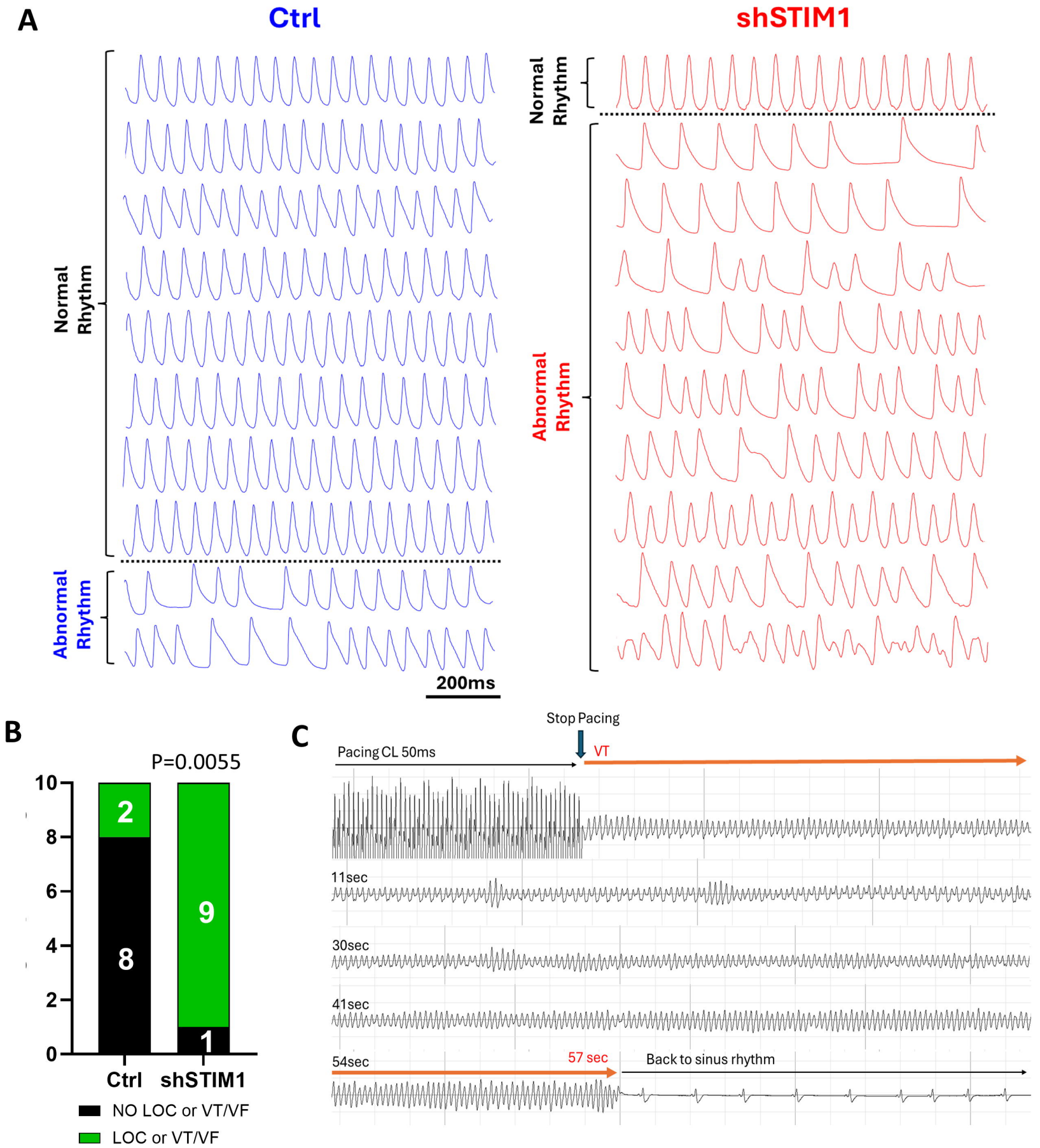
A
Ctrl
shSTIM1
Normal Rhythm
Abnormal Rhythm
Normal Rhythm
Abnormal Rhythm
200ms
B
P=0.0055
10
8
6
4
2
0
2
8
9
1
Ctrl
shSTIM1
NO LOC or VT/VF
LOC or VT/VF
C
Stop Pacing
Pacing CL 50ms
VT
11sec
30sec
41sec
54sec
57 sec
Back to sinus rhythm